Solute Diffusion in Liquid Nickel Measured by Pulsed Ion Beam Melting

J.P. LEONARD, T.J. RENK, M.O. THOMPSON, and M.J. AZIZ

Measurements of liquid-phase diffusion coefficients for dilute tungsten and molybdenum in molten nickel were made using a pulsed ion-beam melting technique. A high-intensity beam of nitrogen ions is focused on the surface of a nickel substrate that was implanted with known concentration profiles of W and Mo. Melting of the surface to a depth of $\sim 1\ \mu$m allows broadening of the implant profiles while molten. Solute concentration-depth profiles were determined before and after melting using Rutherford backscattering spectrometry. Using a series of numerical simulations to estimate the melt history and diffusional broadening for mean liquid temperatures in the range 1755 to 2022 K, an effective diffusion coefficient is determined in each case by comparison to the measured depth profiles. This is found to be $(2.4 \pm 0.2) \times 10^{-5}$ cm^2/s for W and $(1.6 \pm 0.4) \times 10^{-5}$ cm^2/s for Mo, with an additional systematic uncertainty of $\pm 0.5 \times 10^{-5}$ due to instrumental and surface effects.

I. INTRODUCTION

NICKEL alloys have important high-temperature structural applications. Nickel is currently found in over 90 pct of all superalloys used in gas turbine blades, furnace equipment, and power plant components. Nickel is favored because of its high melting temperature, oxidation resistance, and favorable mechanical properties at high temperatures.[1] A wide array of alloy formulations and processing techniques have been developed to meet critical property requirements such as high strength, corrosion resistance, creep, and fatigue resistance. Key to these properties are engineered microstructures, including grain size control and texturing in directionally solidified (or single crystal) components, grain boundary composition control, and the formation and tailoring of secondary phase precipitates and oxide dispersion-strengthened structures.

Process modeling of this complex behavior necessarily requires accurate values of liquid-phase thermophysical properties. In particular, the diffusion coefficient of alloying elements in molten nickel is crucial, yet, as in most liquid metals systems, is lacking.[1] This article reports on measurement of the diffusion coefficients of Mo and W in nickel, which are commonly added for solid solution strengthening. These elements reside in the primary austenitic γ phase, often in concentrations as high as 10 pct.[2] They are also known to react to form carbides of the form MC and upon decomposition M_6C and $M_{23}C_6$, often associated with grain boundaries.

Measurement of diffusion in molten metals is difficult, particularly in refractory and reactive systems.[3] Under ambient terrestrial conditions, these measurements are limited by convective instabilities in the melt, often obscuring diffusive transport. Various capillary and other techniques have been successfully used on low melting temperature metals to limit convection, but they are of limited applicability in refractory and reactive systems, where interactions with capillary walls are more likely. Microgravity experiments can eliminate these effects at great cost, but surface-tension-driven Marangoni convection is often still present.

Pulsed laser beam melting has successfully been used to measure diffusion coefficients in liquid metals, and avoids the limitations of the other techniques.[4,5,6] By inducing uniform melting in a shallow surface layer over a short duration, convection is effectively eliminated. Reactive contamination is also eliminated because the molten pool is contained by identical solid, while reactivity at the free surface is limited by the brief melt duration.

Ion beam melting avoids some limits of laser melting,[7] while maintaining all the advantages of convection and contamination free melting, and has been successfully used in measurement of diffusion coefficients in liquid Ti.[5] Surface melt instabilities are absent as there are no reflection or surface roughness effects. With ion beam melting, the molten layer depth can extend up to 1 μm, resulting in lower temperature gradients that reduce instabilities and potential surface damage. As in pulsed laser melting, melt temperature evolution estimates remain the most challenging aspect, and must be obtained indirectly *via* numerical simulation. Ion beams have the major advantage that the absence of surface reflective effects causes all the incident ion energy to be absorbed, so that the absorbed fluence can be obtained directly from integration of the measured beam current profile.

II. EXPERIMENTAL

Samples were prepared from pure 99.999 pct Ni sheet 0.5-mm thick (Goodfellow), which was cut into bars 25-mm long by 8-mm wide. Following a published procedure for inducing grain growth,[8] the samples were annealed at 850 °C for 96 hours in a vacuum furnace ($p < 10^{-6}$ Torr) in the presence of a reducing charcoal powder. Upon removal, the samples had a bright luster, with a grain size approximately 200 to 400 μm clearly visible under optical microscopy. Samples

J.P. LEONARD, formerly Postdoctoral Researcher, Division of Engineering and Applied Sciences, Harvard University, is Assistant Professor, Materials Science and Engineering, University of Pittsburgh, Pittsburgh, PA 15261. Contact e-mail: jleonard@engr.pitt.edu T.J. RENK, Principal Member of Technical Staff, is with Beam Applications and Initiatives, Sandia National Laboratories, Albuquerque, NM 87185-1182. M.O. THOMPSON, Professor, is with the Materials Science and Engineering Department, Cornell University, Ithaca, NY 14853. M.J. AZIZ, Gordon McKay Professor of Materials Science, is with the Division of Engineering and Applied Sciences, Harvard University, Cambridge, MA 02138.

Manuscript submitted February 25, 2004.

were then polished with conventional metallographic techniques (diamond slurry to 0.25 μm, followed by 0.05-μm colloidal silica), yielding a mirror finish with approximately 80 Å peak-to-valley roughness over a 20-μm lateral distance. These samples were then stored under nitrogen gas until use.

Implantation consisted of 400 keV Mo^{++} ions with a dose of $10^{16}/cm^2$ in one set, and 200 keV W^{++} ions with a dose $5 \times 10^{15}/cm^2$ in the other. This corresponds to peak concentrations of 2.0 pct (657 Å range, 227 Å straggling) and 1.8 pct (245 Å range, 74 Å straggling), respectively. These concentrations are within the solubility range for binary solid solutions of Mo and W in nickel, well outside the range of intermediate solid solutions or intermetallic compounds. Calculations also show these concentrations are below the absolute stability limit for planar solidification[9] at typical resolidification velocities.[10] With both systems in the dilute solution regime, composition-dependent effects on diffusion behavior or thermophysical properties are assumed to be absent—pure nickel is assumed in all subsequent heat flow and solidification modeling.

The melting experiments used an intense pulsed nitrogen ion beam at the RHEPP facility at Sandia National Laboratories, in a configuration shown schematically in Figure 1. This system can produce an intense pulsed beam of nitrogen ions or protons at various energies and fluxes; additional details are provided elsewhere.[7] Fluence was measured by two methods: (1) melt duration of a silicon wafer, which is well calibrated from previous research, placed adjacent to the metal bar; and (2) integration of the ion current (recorded by Faraday cups located on either side of the sample) and energies of the various ion species.

The experiments consisted of melting of the Ni surface using a single pulse consisting primarily of three ion species (H^+, N^+, and N^{++}). The aggregate pulse had a duration of approximately 200 ns and total energy fluence ranging from 1.3 to 1.93 J/cm^2, which resulted in a transient melt of duration of 200-350 ns. Rutherford backscattering spectrometry (RBS) was used to determine the solute depth profile in each sample before and after melting. Backscattering spectra were taken with a normal incidence $4He^{++}$ beam at 3.0 and 4.0 MeV for W- and Mo-implanted samples, respectively, with a near-normal backscattering geometry. No additional channeling or grazing incidence techniques were used.

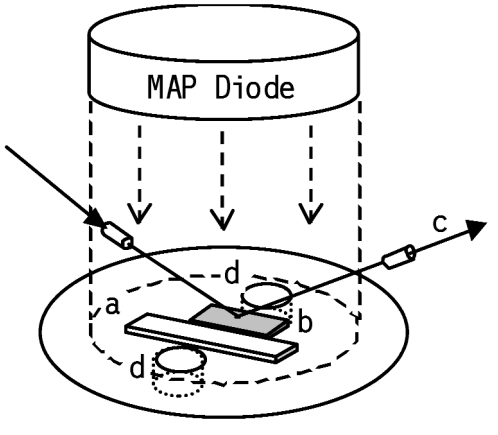

Fig. 1—Schematic view of ion beam melting setup. Ion flux from the magnetically injected anode plasma (MAP) diode is incident on (*a*) the nickel sample and (*b*) the Si calibration sample lying next to it. (*c*) A 660 nm CW diode laser beam delivered through fiber optic lines allows monitoring of the surface reflectivity changes in the Si sample upon melting and solidification to obtain a melt duration for each experiment. Additionally, (*d*) two Faraday cups mounted adjacent to the samples provide a measurement of the beam current and spatial uniformity.

III. DATA ANALYSIS

A. *Concentration Profiles*

The RBS spectra for each sample before and after melting were converted to composition *vs* depth, as shown in Figure 2 by using a calibrated sample consisting of a thin Au film on

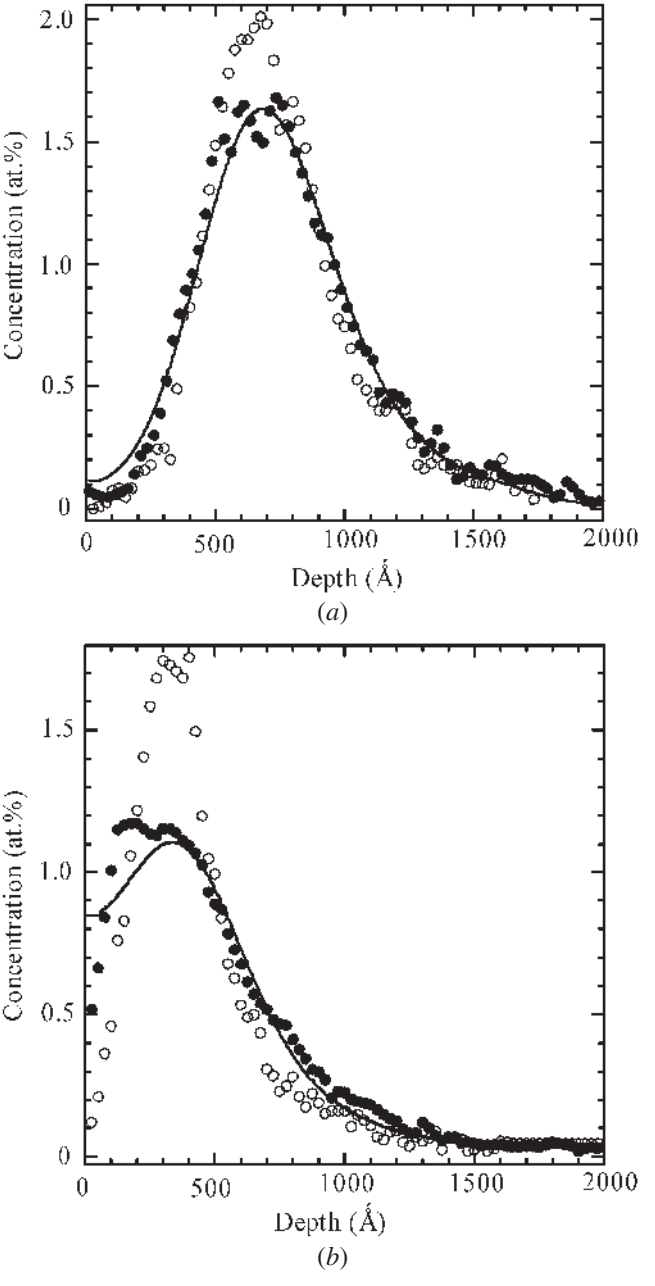

Fig. 2—Typical solute concentration profiles for (*a*) Mo-implanted and (*b*) W-implanted nickel. The open circles are the as-implanted concentration profile, and the solid circles are the diffused profile after melting. The units are the mole fraction, and the solid line is the best-fit profile from numerical calculations.

Si, and a numerical calculation using tabulated energy loss and scattering cross sections.[11] All composition profiles were shifted 100 Å deeper into the film to correct for a systematic error in the RBS energy calibration, as discussed subsequently. In all cases, the W and Mo solute peaks were clearly visible separate from the Ni signal and were reproducible in the as-implanted and postmelted samples. The average solute concentration over the region amenable to numerical analysis was 0.65 at. pct for Mo and 0.52 at. pct for W.

The intrinsic RBS detector resolution was 19 keV, corresponding to a depth resolution of 180 Å and 212 Å in the W- and Mo-implanted samples, respectively. This results in artificially detector-resolution-broadened profiles for all measurements. It occurs identically with respect to both the as-implanted and diffused profiles, and is, to first order, additive with the diffusion broadening.[10] It is therefore possible to determine the amount of diffusional broadening by comparing the detector-resolution-broadened as-implanted and diffused profiles, eliminating the need for deconvolution to remove the detector-resolution broadening, which is in practice very difficult and can lead to systematic errors.

B. *Simulations*

Diffusion coefficients were estimated through a series of numerical simulations. First, the melt and temperature evolution was estimated based on a one-dimensional numerical code "ION" developed for one-dimensional laser melting and rapid solidification[7] but modified to treat the energy deposition characteristics of the pulsed ion beam. Inputs to the code include the total fluence, the thermophysical properties of pure nickel, as shown in Table I, the temporal flux profiles of each ion species (largely N^+, N^{++} and H^+ in this case), their corresponding energies, and the stopping tables.

The estimates of total fluence by the two techniques, given in Table II, show some scatter (± 15 percent) in the relative values, but confirm that the numerical simulations using ION with silicon thermophysical properties were reliable. The fluence values from the integrated Faraday cup flux were used in all subsequent nickel melting simulations, with examples shown in Figure 3. According to the simulations, in all cases, the melt front begins at the surface, sweeps completely through the profile, then returns to the surface upon solidification. Smooth polynomial functions were fit to the melt evolution data in Figure 3(a) to be used as input to the diffusion calculations, while a mean liquid temperature was calculated for each experiment from the node temperature evolution, as shown in Figure 3(b).

A finite-element numerical code "DIFFU" was used to calculate one-dimensional diffusional broadening of as-implanted solute profiles under various melt depth *vs* time conditions using constant values of D_{eff}, the effective diffusion coefficient of the solute in the molten Ni pool. The details are described elsewhere.[5,7] The code is general and assumes diffusion occurs only in the molten region according to a single temperature-independent value of D_{eff}. The calculation does not consider temperature changes nor thermophysical properties of the melt. The segregation coefficient (k) was retained at 1.0 in all simulations, corresponding to partitionless solidification.[5] Given inputs such as the as-implanted profiles in Figure 2, melt history in Figure 3, and D_{eff}, the code generates a broadened profile, which is compared to

Table I. Thermophysical Properties for Nickel Used as Input to the Melt Simulation

Parameter		Value	References
Melting temperature	T_m	1726 K	
Heat of fusion (J/cm^3)	ΔH_{ls}	2654.4	12
Thermal conductivity	$K_{T,\text{sol}}$	$\{0, 0, 149.981, 0.19828, 3.8728 \times 10^{-4}, 7.0954 \times 10^{-8}, -8.1120 \times 10^{-11}\}$*	13
W/(cm K)	$K_{T,\text{liq}}$	$\{0, 0, 0, 0.040335, 3.1463 \times 10^{-4}, -2.8938 \times 10^{-8}, 0\}$*	13, 14
Heat capacity	$C_{p,\text{sol}}$	$\{0, 0, 0, 4.0787, -2.6361 \times 10^{-3}, 7.6635 \times 10^{-6}, 0\}$* ($T < 590$ K)	13
J/(cm^3 K)		$\{0.052875, 19.756, 4746.8, -8.3856, 0.011021, -2.7393 \times 10^{-6}, 0\}$* ($T > 591$ K)	
	$C_{p,\text{liq}}$	5.84	15
Interface response		10.0 m/(s K)	15

*Coefficients of polynomial $c_1T^{-3} + c_2T^{-2} + c_3T^{-1} + c_4 + c_5T + c_6T^2 + c_7T^3$.

Table II. Summary of Results from Experiments and Simulation

		Reflectance		Faraday	Melt Simulation			Diffusion
Sample	Implant	Si Δt_{melt} (ns)	F (J/cm^2)	F (J/cm^2)	T_{mean} (K)	Ni Δt_{melt} (ns)	z_{melt} (nm)	D_{eff} (cm^2/s)
13a	W	1410	1.74	1.71	1947.5	290	649.8	2.60×10^{-5}
13b	W	964	1.43	1.29	1755.1	201	235.8	2.53×10^{-5}
13c	W	1388	1.73	1.75	1961.6	299	678.5	2.08×10^{-5}
19a	Mo	588	1.15	1.29	1755.1	201	235.8	1.60×10^{-5}
19b	Mo	526	1.10	1.34	1783.1	211	299.8	1.26×10^{-5}
19c	Mo	784	1.30	1.43	1825.1	230	399.5	1.35×10^{-5}
20a	Mo	1038	1.49	1.70	1948.3	288	641.9	1.33×10^{-5}
20b	Mo	1108	1.54	1.40	1813.0	224	369.2	2.04×10^{-5}
20c	Mo	1446	1.77	1.65	1925.7	276	603.4	1.56×10^{-5}
22a	Mo	1422	1.75	1.46	1846.5	236	432.7	2.16×10^{-5}
22b	Mo	1792	1.98	1.93	2021.9	342	819.4	1.33×10^{-5}
22c	Mo	2210	2.21	1.89	2008.9	332	790.1	2.05×10^{-5}

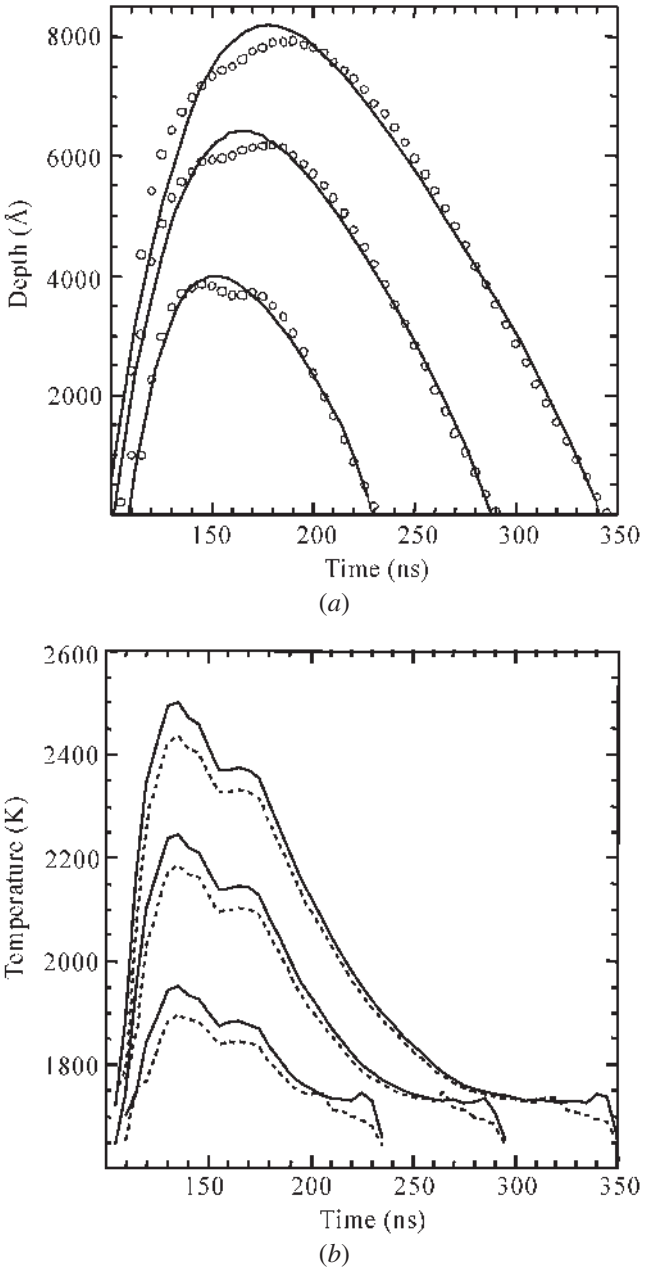

Fig. 3—(*a*) Melt depth evolution for a nickel substrate undergoing pulsed nitrogen ion beam irradiation at, from bottom to top, 1.43, 1.70, and 1.93 J/cm^2, respectively. Solid lines are best-fit polynomial functions to the simulation data. (*b*) Predicted temperature evolution in the melt pool for same, recorded at the surface (solid line) and at 1000 Å depth (dashed lines).

the actual profile after melting. Using a Simplex algorithm, the DIFFU simulations were run for various values of D_{eff} until a best fit of the simulated final profile to the measured final profile was obtained (solid lines in Figure 2).

IV. RESULTS

A summary of the results are given in Table II. Three melting experiments on W-implanted samples, at energies ranging from 1.29 to 1.75 J/cm^2, yielded an effective diffusion coefficient D_{eff} of 2.08 to 2.60 $\times$ 10^{-5} cm^2/s. Nine experiments on Mo-implanted samples yielded lower values of D_{eff}, ranging from 1.33 to 2.16 $\times$ 10^{-5} cm^2/s. The range of liquid temperatures explored is in a relatively narrow range approximately 25 to 295 K above the nickel melting temperature (1726 K), as estimated from the numerical simulations.

V. DISCUSSION

Examination of the data above reveals a scatter in measured diffusivity values for both Mo and W in liquid nickel. This scatter and the limited temperature range of the measurements prevent extraction of the temperature-dependent behavior of D_{eff}, which in liquid metals is expected to increase nearly linearly with temperature.[1,3] This data should therefore be considered a diffusivity measurement for these elements only very near the nickel melting temperature. The observed scatter is likely due to several sources of uncertainty.

A. *Standard Scatter from Errors in Estimation of Fluence*

Estimating the fluence (F) is the largest source of random error. The surface reflectance technique requires estimating a melt duration from a jump in reflectance of a probe laser beam from the surface of silicon, a noisy signal in this current setup. Uncertainties in the true melt duration Δt lead to scatter in estimates of $F(\Delta t)$ generated from ION simulations for Si. Estimates of F from integration of the ion flux are affected by spatial nonuniformities in the ion beam and separation of the Faraday cups from the sample. The remarkable agreement within 15 pct for all estimates not only indicates the validity of these independent techniques (which have no free parameters), but also provides a good estimate of the standard uncertainty in D_{eff}, corresponding to $\pm 0.17 \times 10^{-5}$ and $\pm 0.30 \times 10^{-5}$ cm^2/s for W and Mo, respectively.

B. *Determination of Composition from RBS Profiles*

Concentration profiles before and after are calculated directly from RBS spectra, which rely on the detector energy calibration and include broadening by the detector resolution. In all calculations discussed here, a 100 Å offset was applied to all profiles to correct for an apparent error in the energy calibration. With the offset, the measured profile peak positions were in good agreement with predictions by SRIM,[16] and reduced the effects of instrument broadening in the diffusion calculations for the near-surface region. It is possible that a surface oxide may have been present, which could have shifted the RBS spectra or inhibited diffusion toward the surface. This can be seen in the discrepancy in the calculated diffusion profiles in the first 200 Å of each profile in Figure 2. Calculations indicate this effect may result in a systematic overestimation of D_{eff} of up to 0.5 $\times$ 10^{-5} cm^2/s.

C. *Other Sources of Uncertainty*

The algorithm used to determine the value of D_{eff} giving best agreement with the experiment minimizes a chi-squared error with respect to the RBS concentration profile. In all cases, the estimated random uncertainty is less than 0.1 $\times$

10^{-6} cm^2/s. The ion-beam-melted samples showed minimal surface damage or roughening, and the RBS concentration profiles were consistent with melting through the implant profile followed by uniform resolidification without segregation. Variations in melt pool temperatures from the simulation were found to be about 50 K from top to bottom, while uncertainties in T_{mean} associated with errors in the fluence estimate and thermophysical properties are expected to be about 20 and 100 K, respectively. Convective contamination is expected to be negligible, based on calculations performed for pulsed ion beam melting of other metals.[4]

VI. SUMMARY

Measurements of diffusion coefficients for dilute W and Mo in molten nickel were made using a pulsed ion-beam melting technique and numerical simulation for mean liquid temperatures in the range 1755 to 2022 K. This gives an estimate of $(2.4 \pm 0.2) \times 10^{-5}$ cm^2/s for 0.52 at. pct W and $(1.6 \pm 0.4) \times 10^{-5}$ cm^2/s for 0.65 at. pct Mo. There may be an additional systematic uncertainty of $\pm 0.5 \times 10^{-5}$ cm^2/s due to errors associated with calculating profiles from the RBS spectra. These measurements demonstrate the effectiveness of pulsed ion beam melting for measuring diffusivities in refractory or reactive melts.

This research was supported by NASA grant NAG8-1680.

REFERENCES

1. F.J. Cherne, M.I. Baskes, and P.A. Deymier: *Phys. Rev. B,* 2002, vol. 65, p. 024209; *Phys. Rev. B,* 2002, vol. 66, p. 149902.
2. *Heat-Resistant Materials,* ASM Handbooks, J.R. Davis, ed., ASM, Materials Park, OH, 1997.
3. T. Iida and R.I.L. Guthrie: *The Physical Properties of Liquid Metals,* Clarendon Press, Oxford, 1988.
4. N. Isono, P.M. Smith, D. Turnbull, and M.J. Aziz: *Metall. Mater. Trans. A,* 1996, vol. 27A, pp. 725-30.
5. P.G. Sanders, M.O. Thompson, T.J. Renk, and M.J. Aziz: *Metall. Mater. Trans. A,* 2001, vol. 32A, pp. 2969-74.
6. P.G. Sanders and M.J. Aziz: *J. Appl. Phys.,* 1999, vol. 86, pp. 4258-61.
7. M.O. Thompson and T.J. Renk: *Mater. Res. Soc. Symp. Proc.,* 1998, vol. 504, pp. 33-38.
8. P. Feltham: *J. Inst. Met.,* 1957, vol. 86, pp. 95-97.
9. D.E. Hoglund, M.O. Thompson, and M.J. Aziz: *Phys. Rev. B,* 1998, vol. 58, pp. 189-99.
10. C.B. Arnold, M.J. Aziz, M. Schwarz, and D.M. Herlach: *Phys. Rev. B,* 1999, vol. 59, pp. 334-43.
11. L.C. Feldman and J.W. Mayer: *Fundamentals of Surface and Thin Film Analysis,* North-Holland, NY, 1986.
12. R. Hultgren, R.L. Orr, P.D. Anderson, and K.K. Kelley: *Selected Values of Thermodynamic Properties of Metals and Alloys,* John Wiley & Sons, New York, NY, 1963.
13. *Thermal Properties of Matter,* Y.S. Touloukian, ed., Plenum, New York, NY, 1970.
14. B.J. Monaghan, K.C. Mills, and B.J. Keene: *High Temp. High Pressure,* 1998, vol. 30, pp. 457-64.
15. H.A. Atwater, J.A. West, P.M. Smith, M.J. Aziz, J.Y. Tsao, P.S. Peercy, and M.O. Thompson: *Mater. Res. Soc. Symp. Proc.,* 1990, vol. 157, pp. 369-75.
16. J.F. Ziegler and J.P. Biersack: *SRIM. The Stopping and Range of Ions in Matter,* Version 2000.40.